El Cezeri
Journal of Science and Engineering
ISSN: 2148-3736

Research Article

Thermodynamic and Optimization Comparison of a Solar-Powered Compressor-Assisted Combined Absorption Refrigeration and Power Systems

Chinedu F. Okwose[1a], Mustafa Tunay[1b], Muhammad Abid[2c], Michael Adedeji[3d], Victor Adebayo[3e], Tahir A H. Ratlamwala[4f], Muhammad A. Rabbani[1g]

[1] Faculty of Engineering, Cyprus Science University, Ozankoy-Girne, via Mersin 10, Turkey
[2] Department of Energy Systems Engineering, Faculty of Integrated Technologies, Brunei Darussalam University, Jalan Tungku Link BE 1410, Bandar Seri Begawan, Brunei Darussalam
[3] Department of Energy System Engineering, International Cyprus University, Haspolat-Lefkosa Via Mersin, Turkey
[4] Department of Engineering Science, National University of Sciences and Technology, Karachi, Pakistan

mustafatunay@csu.edu.tr

DOI : 10.31202/ecjse.1434603
Received: 09.02.2024 Accepted: 22.05.2024
How to cite this article:
Chinedu F. Okwose, Mustafa Tunay, Muhammad Abid, Michael Adedeji, Victor Adebayo,Tahir A H. Ratlamwala,Muhammad A. Rabbani, " Thermodynamic and Optimization Comparison of a Solar-Powered Compressor-Assisted Combined Absorption Refrigeration and Power Systems ", El-Cezeri Journal of Science and Engineering, Vol: 11, Iss: 3, (2024), pp.(267-282).
ORCID: [a]0000-0003-0827-4578; [b]0000-0001-8843-621X; [c]0000-0001-6579-6212; [d]0000-0002-7532-3563; [e]0000-0002-9237-7678; [f]0000-0003-3314-5807; [g]0000-0002-0980-5054.

Abstract : The operation and performance of three different combined absorption refrigeration and power systems is presented in this study. The systems are based on the single, double, and triple effect absorption refrigeration cycles with ammonia-water as working fluid pairs all powered by solar thermal energy. The thermodynamic performance of these modified combined absorption cycles have been analyzed for typical thermal boundary conditions and design parameters. The simulation results show that when the compressor pressure ratio increases from 1 to 2, the heat source inlet temperatures can be reduced by 27% ($111.3°C$ to $81.1°C$) in the single effect system, 16% ($182.1°C$ to $152.5°C$ in the double effect system, and 34% ($228.3°C$ to $150.3°C$) in the triple effect system. The exergy efficiency of the triple effect system increases from 38% to 64% for a 75-kW cooling load system. These proposed systems provide a better way to optimise the utilisation of heat sources with moderate temperatures.

Keywords : Absorption Refrigeration, Compression Ratio, Power, Cooling, Triple Effect

1 Introduction

The cooling & refrigeration needs in many countries keep increasing as a consequence of global warming experienced worldwide [1]. This increasing requirement for comfort & high cooling loads needs to be met using environmentally responsible means to prevent further damage to the earth's atmosphere. An example of such an option is cooling and refrigeration using vapor absorption systems. Unlike popular and commercially available vapor compression systems, vapor absorption systems don't make use of chlorofluorocarbon (CFC) and hydrofluorocarbon (HCFC) refrigerants that can cause the ozone layer depletion and also act to trap heat in the lower atmosphere leading to climate change [2]–[5] This makes absorption cooling and refrigeration systems more environmentally friendly in comparison. Additionally, they can be powered by waste low grade heat thereby greatly reducing their electricity usage [6].

Several working fluids are used in vapor absorption systems which all have different input conditions and advantages. Hugo et al. [7] investigated the performance of six different working fluid pairs used in absorption refrigeration systems. The working fluid pairs considered are H_2O-LiBr, NH_3-H_2O, NH_3-$LiNO_3$, NH_3-NaSCN, H_2O-LiCl, and H_2O-$CaCl_2$. They found in their study that the fluid pairs that use H_2O as the refrigerant are more efficient compared to the ones utilizing NH_3 as the refrigerant. However, water as the refrigerant will make sub-zero cooling/refrigeration impossible because it will freeze at said temperature ($0°C$). Ammonia as the refrigerant in a working fluid pair on the other hand allows sub-zero cooling.

The inlet temperature of the heat supplied to the generator of the system from an external source is a vital factor in the operation of absorption cooling systems. The driving heat of the system is needed for fluid separation in the generator/desorber. This inlet heat temperature is thus dependent on the type of working fluid pair in the system and also the number of stages of separation. For instance, single effect LiBr-H_2O systems require heat at about $70°C$ while the double and triple-effect systems require about $150°C$ and $200°C$ respectively. NH_3-H_2O systems require higher temperatures in comparison; the single effect systems operate at about $90°C$, the double effect systems at about $170°C$, and the triple effect systems at over $200°C$ [8]–[10].

In a bid to reduce the minimum operating temperatures of vapor absorption systems, researchers developed a model that incorporates a compressor into the system. The compressor can be placed between the evaporator and the absorber or between the generator and the condenser [11], [12]. Shu et al. [6] found that the generator temperature of a triple effect NH_3-H_2O cooling system can be reduced by up to $50°C$ when coupled with a compressor. Chen et al. [13] examined the operational efficiency of a compressor-assisted double-effect absorption refrigeration system. This system which uses a [mmim] DMP/CH_3OH working fluid exhibited its best performance when a compressor is placed between the evaporator and absorber. Their study also showed that placing the compressor between the two generators is an acceptable configuration option. According to Boer et al. [14], placing a compressor between the evaporator and the absorber has many functions. These include increasing the deflation range, increasing absorption temperature, and decreasing generation temperature.

In addition to reducing the inlet heat temperature requirement in absorption cooling systems, the introduction of the compressor also increases the performance. However, the additional compression work of the system needs to be considered. There have already been numerous researches conducted on absorption cycles that include a turbine/expander for cogeneration of cooling and power.

Demirkaya et al. [15] examined the Goswami cycle, which integrates power generation and cooling using NH_3-H_2O. Praveen Kumar et al. [16] explored the impact of operational temperatures on a combined cycle involving ammonia absorption refrigeration (AAR) and the Kalina cycle. They reported the system's effective first law and exergy efficiencies as 13% and 48%, respectively. Shu et al. [6] conducted a simulation to assess the thermal performance of a proposed compressor-assisted triple-effect LiBr/H_2O absorption cooling cycle coupled with a Rankine cycle driven by high-temperature waste heat. Their findings demonstrated that the integrated compressor enhances the thermal efficiency of multi-effect absorption refrigeration. The development of these combined cooling and power cycles makes it possible to have a hybrid compressor-assisted absorption cooling system that is capable of generating the needed compression work in the system. These self-sufficient compressor-aided systems have been the subject of various research. Agheniaey et al. [17] obtained a second law efficiency of 11.56% in their study of a novel absorption refrigeration cycle with an expander and compressor. Ayou et al. [18] also performed a study on an integrated compressor booster for a power and refrigeration cycle. Their system is a modified single effect NH_3-H_2O cycle which they showed can conveniently operate in 3 distinct modes; cooling, power, and coproduction. In their research, Chinedu et al. [19] conducted a study on a compressor-assisted two-stage triple-effect absorption cycle designed for both power generation and cooling purposes. This system consists of a power sub-system and an absorption-compressor sub-system, with ammonia-water mixture as the working fluid.

Chinedu et al. [20] demonstrated that the inlet temperature of the heat source was reduced by $50°C$ compared to the traditional two-stage triple-effect absorption system. They investigated compressor-assisted single, double, and triple-effect absorption refrigeration cycles for power and cooling using thermal energy from evacuated tube collectors. Their findings indicate that the net power output decreased by 88%, while the cooling output increased slightly by 5.2% for the single-effect cycle.

The research on the hybrid compressor-assisted vapor absorption NH_3-H_2O systems for cooling and power generation has all been focused on the single effect cycles. There appears to be no study available on multi-effect compressor-assisted vapor absorption NH_3-H_2O systems for cooling and power generation. This paper therefore aims to fill this gap by providing an analysis of NH_3-H_2O double, and triple-effect systems working according to this configuration. This study investigates the operation and performance of three combined absorption refrigeration and power systems utilizing solar thermal energy. The systems are based on single, double, and triple-effect absorption refrigeration cycles, employing ammonia-water as the working fluid pairs. Through analysis of thermodynamic performance under typical thermal boundary conditions and design parameters, the study evaluates the modified combined absorption cycles. Also, it will be simulated using the engineering equation solver (EES) tool. The performance characteristics will be assessed by increasing the pressure ratio (Prcom) of each system from 1 to 2, according to the given input conditions.

2 Unit Description and Working Principle

This section describes the three systems considered in this study. Each of the systems is based on the typical single effect, two-stage double-effect and two-stage triple-effect NH_3/H_2O vapor absorption cycles extensively described in [21]. Two-stage ammonia/water absorption systems offer the potential for increased efficiency (coefficient of performance) or increased temperature lift (difference between lowest temperature and the heat rejection temperature) compared to single-stage cycles. They are basically two single effect systems; Two-stage implies that two solution circuits are included in the system and double/triple effect implies that a certain amount of heat is used more than once to generate refrigerant vapor. In each of the systems, the term "strong solution" represents a solution that is strong with refrigerant (NH_3), while "weak solution" represents a solution that is weak with refrigerant.

2.1 Single Effect Combined Absorption Refrigeration and Power (SECARP) System

The main components of the SECARP are: generator, condenser, evaporator, absorber, expander, solution pump, superheater, rectifier, and solution heat exchanger. The evaporator works at the low pressure of the system, the absorber works at the

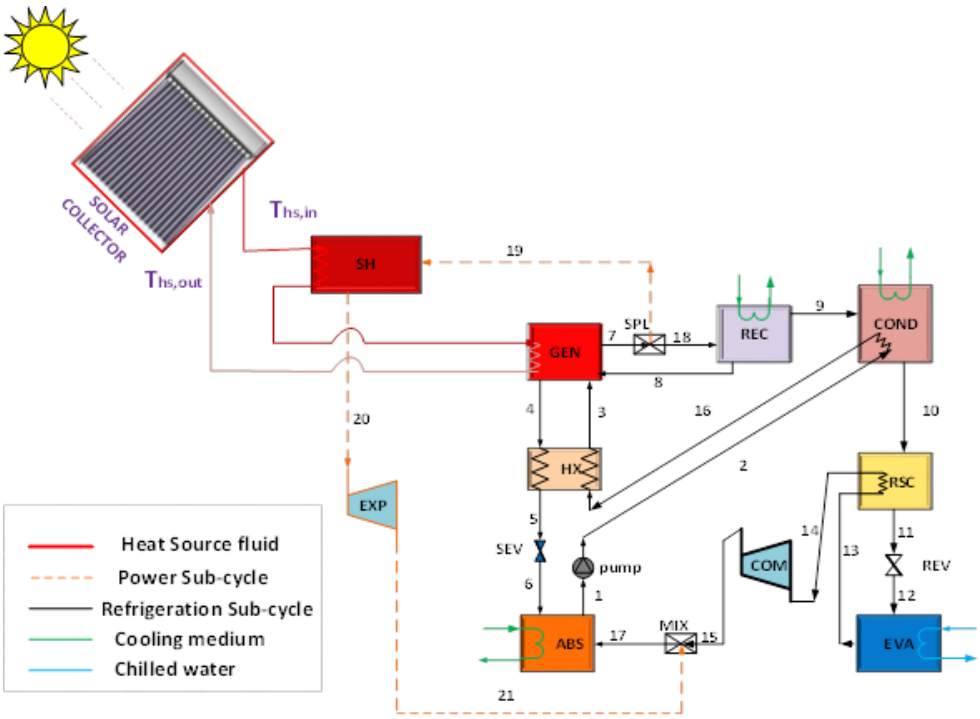

Figure 1: The Solar Powered SECARP Cycle

intermediate pressure while the generator, superheater, & condenser work at the high pressure.

In the SECARP system shown in Fig. 1, the sub-cooled solution leaving the absorber at state 1 enters the solution pump which increases its pressure from the intermediate pressure to the high pressure leaving at state 2. The high-pressure strong solution then passes through the heat exchanger where it exchanges heat with the high temperature water coming from the generator (state 4). The solution then leaves at a higher temperature at state 3 and enters the generator. Heat from an external source is introduced into the generator, raising the temperature of the solution until the boiling point of ammonia is reached. This causes the ammonia in the solution to evaporate leaving behind the water. The ammonia at state 7 exiting the generator will however still contain a small concentration of water, this is because of how close the boiling points of both ammonia and water are. If this ammonia refrigerant containing a small quantity of water is passed into the evaporator, it will likely cause problems for the evaporator. A rectifier is used to extract the remnant water from the ammonia and this water (state 8) is passed back into the generator.

The ammonia refrigerant vapor is then passed into the condenser and leaves as a condensed liquid at state 10. The refrigerant now flows into the refrigerant sub-cooler (RSC) where it is pre-cooled before it flows out (state 11) into the refrigerant expansion valve (REV). It is then throttled in the to reduce the pressure which will also lead to a drop in its temperature. The low temperature refrigerant (state 12) now proceeds into the evaporator (EVA), which is where the cooling happens. This is achieved by passing heat from the space/water that needs cooling into the evaporator. The refrigerant at state 13, after leaving the evaporator, then passes through the REV where it provides the cooling required for the initial pre-cooling in the REV. This same process will also ensure that the emerging refrigerant at state 14 is at a superheated vapor state, which then goes through the compressor to increase its pressure to that of the absorber.

In the SECARP system shown in Fig. 1, the sub-cooled solution leaving the absorber at state 1 enters the solution pump which increases its pressure from the intermediate pressure to the high pressure leaving at state 2. The high-pressure strong solution then passes through the heat exchanger where it exchanges heat with the high temperature water coming from the generator (state 4). The solution then leaves at a higher temperature at state 3 and enters the generator. Heat from an external source is introduced into the generator, raising the temperature of the solution until the boiling point of ammonia is reached. This causes the ammonia in the solution to evaporate leaving behind the water. The ammonia at state 7 exiting the generator will however still contain a small concentration of water, this is because of how close the boiling points of both ammonia and water are. If this ammonia refrigerant containing a small quantity of water is passed into the evaporator, it will likely cause problems for the evaporator. A rectifier is used to extract the remnant water from the ammonia and this water (state 8) is passed back into the generator.

The ammonia refrigerant vapor is then passed into the condenser and leaves as a condensed liquid at state 10. The refrigerant now flows into the refrigerant sub-cooler (RSC) where it is pre-cooled before it flows out (state 11) into the refrigerant expansion

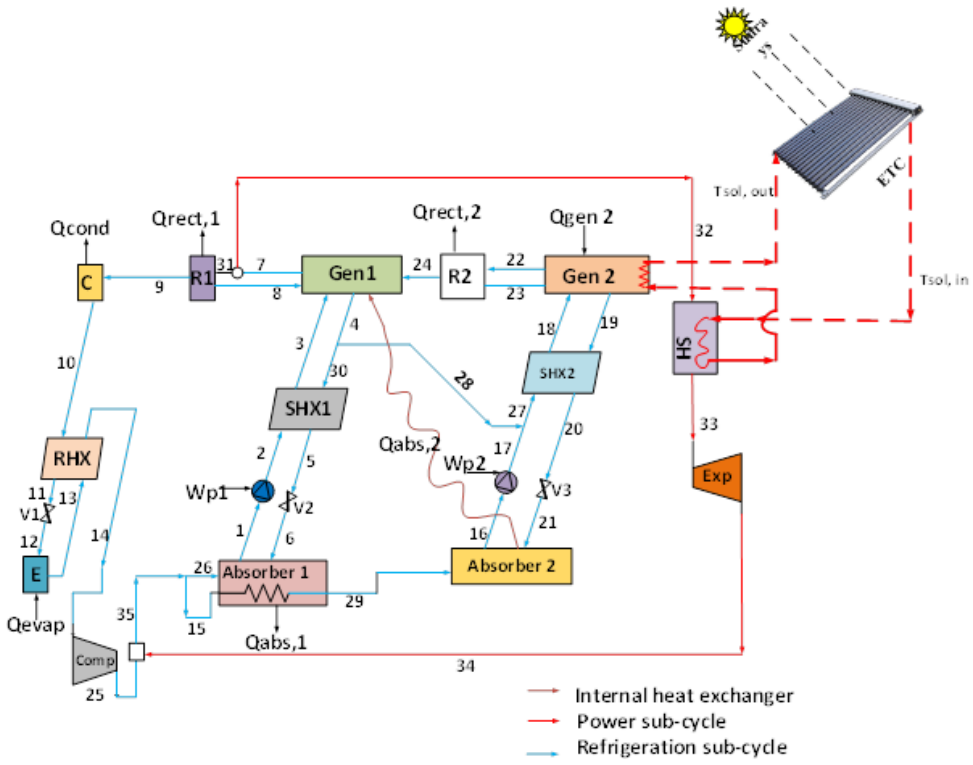

Figure 2: The Solar Powered DECARP Cycle

valve (REV). It is then throttled in the to reduce the pressure which will also lead to a drop in its temperature. The low temperature refrigerant (state 12) now proceeds into the evaporator (EVA) where the cooling effect occurs. This is achieved by passing heat from the space/water that needs cooling into the evaporator. The refrigerant at state 13, after leaving the evaporator, then passes through the REV where it provides the cooling required for the initial pre-cooling in the REV. This same process will also ensure that the emerging refrigerant at state 14 is in a superheated vapor state, which then goes through the compressor to increase its pressure to that of the absorber.

After leaving the generator at state 7, a portion of the refrigerant is separated (state 19) and is passed into the superheater (SH). Here, heat from the external source (evacuated tube solar collector) is used to raise the temperature of the refrigerant until it becomes a superheated vapor. This then goes into the expander (state 20) where it expands, creating mechanical work. The refrigerant exiting the expander (state 21) mixes with that leaving the compressor forming state 17 which flows into the absorber.

The weak solution (water) leaving at state 4, after exchanging heat with the strong solution (state 3) in the SHX, flows through the solution expansion valve (SEV) which will reduce its pressure to that of the absorber. The weak solution and the refrigerant are then mixed in the absorber when the absorber heat (Qabs) rejected.

2.2 Double Effect Combined Absorption Refrigeration and Power (DECARP) System

The DECARP system shown in Fig. 2 consists of two single effect absorption cycles working in tandem and the process of fluid separation is done in 2 generators operating at the same pressure. The left stage of the system is identical to the SECARP system and also undergoes the same processes from states 1 to 14. The second stage consists of the absorber2, pump2, solution heat exchanger2, generator2, and rectifier2.

The combination of the heat rejected from absorber2 and rectifier2 is supplied to generator1 to aid fluid separation. The refrigerant emerging from rectifier2 (state 24) is mixed with the strong solution (state 3) in generator1. After the separation in generator1, a portion of the weak solution (state 4) is extracted and mixed with the state 17. The mixture (state 27) then passes through SHX2 where it gains heat which increases its temperature before flowing into generator2. The refrigerant utilized for power generation in the system is extracted from the stream leaving generator1 (state 7). This ensures that a sufficient amount of the refrigerant is available before the separation making it possible to have power generation even with a low refrigerant split ratio.

The portion of the refrigerant that goes into cooling in the evaporator leaves the RHX at state 14 and then goes into the compressor. The compressed refrigerant then mixes with the refrigerant leaving the expander and the mixture (state 35) is then

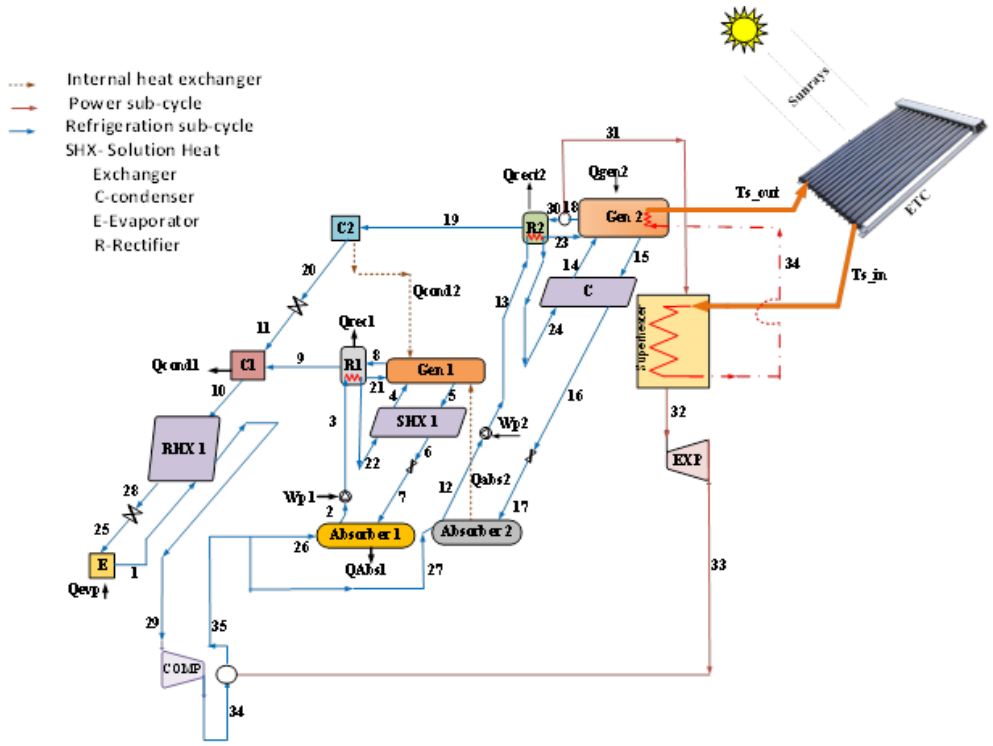

Figure 3: The Solar Powered TECARP Cycle

shared into both absorbers. The share of the refrigerants flowing into absorber2 (state 15) is first passed through absorber1 without mixing. Here, it gains heat which increases its temperature before finally flowing into absorber 2.

2.3 Triple effect combined absorption refrigeration and power (TECARP) system

Fig.3 shows the TECARP cycle which uses rejected heat from a coupled high-pressure single effect cycle to drive an inner stage single effect cycle. Similar to the DECARP cycle, it also comprises two generators for fluid separation and two absorbers for reabsorption. The difference however is that the inner and outer stages operate at different generator temperatures. The pressure of the outer stage generator is higher than that of the inner stage which means that each stage will have its separate condenser. The heat required by the generator of the inner cycle is provided by a combination of the Thermal energy rejected in the outer stage generator and absorber.

The refrigerant from rectifier 2 (state 19) is passed into condenser 2. The emerging saturated refrigerant (state 20) then passes through an expansion valve which reduces its pressure to that of condenser 1. Here, it mixes with the refrigerant exiting rectifier 1 and the mixture is then condensed and leaves at state 10.

The same process of refrigerant extraction also occurs in the TECARP cycle. A portion of the refrigerant leaving the outer stage generator is extracted (state 31) and passed through the superheater. The high temperature refrigerant (state 32) expands in the expander chamber consequently generating the power in the system. The refrigerant leaving the evaporator (state 1) after going through the RHX is passed through the compressor which increases its pressure according to the Prcom. After leaving the compressor, the compressed refrigerant (state 34) mixes with the refrigerant exiting the expander (state 33) and the resultant mixture (state 35) is separated into two streams; one flowing into absorber 1 (state 26) and the other flowing into absorber 2 (state 27).

3 The System Modelling

In the following section, equations based on the mass, concentration, energy, and exergy balance of each component of the three cycles are presented. The equations governing the first and second law performance of the systems are also presented. Tables 1-3 give the energy and exergy balance equations used for the thermodynamic analysis of each component in the three systems analyzed and calculate the exergy destruction rate of each constituent, the exergy at every state point should be defined. Also, chemical and physical exergy was included. The specific physical exergy at every state point (Table 3) is given as [22]:

$$ex_{ph.i} = (h_1 - h_0) - T_0(s_i - s_0) \quad (1)$$

where h_0 and s_0 are the specific enthalpy and entropy for a temperature of $25°C$ and Pressure of 101.3 kPa. The specific chemical exergy of the ammonia water at each state point is expressed as [23]:

$$ex_{ch.i} = \frac{z_i}{M_{NH_3}} e^0_{ch.NH_3} + \frac{1 - z_i}{M_{H_2O}} e^0_{ch.H_2O} \tag{2}$$

where $e^0_{ch.NH_3}$ and $e^0_{ch.H_2O}$ are the normal molar specific exergies of NH_3 and H_2O, M is molar mass. At each state point,the overall specific exergy is expressed as [24]:

$$ex_i = ex_{ph.i} + ex_{ch.i} \tag{3}$$

The cycle steady-state flow exergy balance equation is [25]:

$$\sum_{i \epsilon IN(u)} ex_i m_i^{\cdot} - \sum_{i \epsilon OUT(u)} ex_i m_i^{\cdot} + \tau_u Q_u^{\cdot} - W_u^{\cdot} = E^{\cdot} x_{D.u} \tag{4}$$

The exergy flow related to inlet and outlet mass flow are the first two terms on the left. Where $Q_u^{\cdot}$ and $W_u^{\cdot}$ are the heat and work transfer rates that go in and out of the system and $E^{\cdot} x_{D.u}$ is the unit exergy destruction rate. The cycle energy efficiency (η_1) is given as [26]:

$$\eta_1 = \frac{W_{net}^{\cdot} + Q_{cold}^{\cdot}}{Q_{gen2}^{\cdot} + Q_{sh}^{\cdot}} \tag{5}$$

where $W_{net}^{\cdot}$ is the expander output power minus the pump and compressor work, $Q_{des2}^{\cdot}$ and $Q_{sh}^{\cdot}$ are the desorber and super heater heat input.

The exergy efficiency (η_{ex}) of the combined cycle are [18]:

$$\eta_{ex} = \frac{W_{net}^{\cdot} + E^{\cdot} x_{cold}}{E^{\cdot} x_{gen2} + E^{\cdot} x_{sh}} \tag{6}$$

Combined absorption cycles for dual-production have separate thermodynamic quality, which is not comparable in adding them to the performance evaluation criteria. Therefore, energetic and exergetic performance indicators should, therefore, be considered based on the thermodynamic quality of the useful outputs. In order to evaluate the cooling output of the cycle, the exergy of the cold output should be split by a practical second-law efficiency $(\eta_{II,ref})$ for vapor compression refrigeration cycles. The effective energy and effective exergy efficiency are given as [16], [18]:

$$\eta_{I,eff} = \frac{W_{net}^{\cdot} + \frac{E^{\cdot} x_{cold}}{\eta_{II,ref}}}{Q_{gen2}^{\cdot} + Q_{sh}^{\cdot}} \tag{7}$$

$$\eta_{ex,eff} = \frac{W_{net}^{\cdot} + \frac{E^{\cdot} x_{cold}}{\eta_{II,ref}}}{E^{\cdot} x_{gen2} + E^{\cdot} x_{sh}} \tag{8}$$

The total exergy destruction rate $(E^{\cdot} x_{D,total})$ represents the lost work potential of driving thermal energy and should be minimised. It can be calculated by adding the sum of individual unit exergy destruction rates. The non-dimensional exergy destruction in each unit is the ratio of its exergy destruction to the cycle's total exergy destruction: $(E^{\cdot} x_{D,u})/(E^{\cdot} x_{D,total})$.

In order to analyze the performance of the different absorption cooling systems, the following assumptions have been made:

- The analysis is made under steady state conditions.
- NH_3 -H_2O solution is at saturated state when leaving the generator & absorber, and refrigerant is at a saturated state when leaving condenser & evaporator.
- Heat losses & pressure drops in the components are negligible.
- The pump process & pressure reduction in the valves are adiabatic.
- The refrigerant vapour concentration at rectifier exits is 0.999.

The design parameters considered for the 3 systems are presented in Table 4. For the purpose of comparison, these parameters are used in all the systems. The refrigerant separation ratio (RSR) determines the amount of the refrigerant that will be passed to the expander for power production and the solution circulation ratio (SCR) is defined as the ratio of the strong solution flow rate to the refrigerant flow rate [27].

Table 1: Energy and Exergy Destruction Equations for the SECARP System

Component	Energy is Different from Exergy	Exergy Balance
Pump	$W_p = m_1(h_2 - h_1)$	$E \cdot x_1 + W_p = E \cdot x_2 + E \cdot x_{dest.pump}$
Solution heat exchanger	$m_4 h_4 + m_{16} h_{16} = m_3 h_3 + m_5 h_5$	$E \cdot x_4 + E \cdot x_{16} = E \cdot x_3 + E \cdot x_5 + E \cdot x_{dest.shx}$
Absorber	$m_6 h_6 + m_{17} h_{17} = m_1 h_1 + Q_{Abs}$	$E \cdot x_6 + E \cdot x_{17} + E \cdot x_{cw2.in} = E \cdot x_1 + E \cdot x_{cw2.out} + E \cdot x_{dest.Abs}$
Generator	$m_3 h_3 + m_8 h_8 = m_7 h_7 + Q_{Gen}$	$E \cdot x_3 + E \cdot x_8 = E \cdot x_7 + E \cdot x_{dest.Gen}$
Condenser	$Q_{con} = m_9(h_9 - h_{10})$	$E \cdot x_9 + E \cdot x_{cw1.in} = E \cdot x_{10} + E \cdot x_{cw1.out} + E \cdot x_{dest.con}$
Rectifier	$m_{18} h_{18} = m_8 h_8 + m_9 h_9 + Q_{Rec}$	$E \cdot x_{18} = E \cdot x_8 + E \cdot x_9 + E \cdot x_{dest.Rec}$
Evaporator	$Q_{Eva} = m_{13}(h_{13} - h_{12})$	$E \cdot x_{12} + E \cdot x_{cf.in} = E \cdot x_{13} + E \cdot x_{cf.out} + E \cdot x_{dest.Eva}$
Refrigerant sub-cooler	$m_{10} h_{10} + m_{13} h_{13} = m_{11} h_{11} + m_{14} h_{14}$	$E \cdot x_{10} + E \cdot x_{13} = E \cdot x_{11} + E \cdot x_{14} + E \cdot x_{dest.Rsc}$
Expander	$W_{Exp} = m_{20}(h_{20} - h_{21})$	$E \cdot x_{20} = E \cdot x_{21} + W_{Exp} + E \cdot x_{dest.Exp}$
Compressor	$W_{Com} = m_{14}(h_{15} - h_{14})$	$E \cdot x_{14} + W_{Com} = E \cdot x_{15} + E \cdot x_{dest.Com}$
Super heater	$Q_{sh} = m_{19}(h_{20} - h_{19})$	$E \cdot x_{19} + E \cdot x_{hs.in} = E \cdot x_{20} + E \cdot x_{hs.int} + E \cdot x_{dest.sh}$

Table 2: Energy and Exergy Destruction Equations for the DECARP System

Component	Energy is Different from Exergy	Exergy Balance
Pump 1	$W_{p1} = m_1(h_2 - h_1)$	$E \cdot x_1 + W_{p1} = E \cdot x_2 + E \cdot x_{dest.pump1}$
Solution heat exchanger 1	$m_2 h_2 + m_{30} h_{30} = m_3 h_3 + m_5 h_5$	$E \cdot x_2 + E \cdot x_{30} = E \cdot x_3 + E \cdot x_5 + E \cdot x_{dest.shx1}$
Absorber 1	$m_6 h_6 + m_{15} h_{15} + m_{26} h_{26} = m_1 h_1 + m_{29} h_{29} + Q_{Abs1}$	$E \cdot x_6 + E \cdot x_{15} + E \cdot x_{26} + E \cdot x_{cw2.in} = E \cdot x_1 + E \cdot x_{29} + E \cdot x_{cw2.out} + E \cdot x_{dest.Abs1}$
Generator 1	$m_3 h_3 + m_8 h_8 + m_{24} h_{24} + Q_{Rec2} + QAbs2 = m_4 h_4 + m_7 h_7 + Q_{Gen1}$	$E \cdot x_3 + E \cdot x_8 + E \cdot x_2 4 + E \cdot x_{Rec2} + E \cdot x_{Abs2} = E \cdot x_4 + E \cdot x_7 + E \cdot x_{dest.Gen1}$
Pump 2	$W_{p2} = m_{16}(h_{17} - h_{16})$	$E \cdot x_{16} + W_{p2} = E \cdot x_{17} + E \cdot x_{dest.pump2}$
Solution heat exchanger 2	$m_{19} h_{19} + m_{27} h_{27} = m_{18} h_{18} + m_{20} h_{20}$	$E \cdot x_{19} + E \cdot x_{27} = E \cdot x_{18} + E \cdot x_{20} + E \cdot x_{dest.shx2}$
Generator 2	$m_{18} h_{18} + m_{23} h_{23} + m_{sh} h_{hs.int} = m_{19} h_{19} + m_{22} h_{22} + m_{sh} h_{hs.out} + Q_{Gen2}$	$E \cdot x_{18} + E \cdot x_{23} + E \cdot x_{hs.int} = E_{19} + m_{22} + E \cdot x_{hs.out} + E \cdot x_{dest.Gen2}$
Condenser	$Q_{con2} = m_9(h_9 - h_{10})$	$E \cdot x_9 + E \cdot x_{cw1.in} = E \cdot x_{10} + E \cdot x_{cw1.out} + E \cdot x_{dest.con2}$
Rectifier 1	$m_{31} h_{31} = m_8 h_8 + m_9 h_9 + Q_{Rec1}$	$E \cdot x_{31} = E \cdot x_8 + E \cdot x_9 + E \cdot x_{dest.Rec1}$
Rectifier 2	$m_{22} h_{22} = m_{23} h_{23} + m_{24} h_{24} + Q_{Rec2}$	$E \cdot x_{22} = E \cdot x_{23} + E \cdot x_{24} + E \cdot x_{dest.Rec2}$
Absorber 2	$m_{21} h_{21} + m_{29} h_{29} = m_{16} h_{16} + Q_{Abs1}$	$E \cdot x_{21} + E \cdot x_{29} + E \cdot x_{cw3.in} = E \cdot x_{16} + E \cdot x_{cw3.out} + E \cdot x_{dest.Abs2}$
Super heater	$Q_{sh} = m_{32}(h_{33} - h_{32})$	$E \cdot x_{32} + E \cdot x_{hs.in} = E \cdot x_{33} + E \cdot x_{hs.int} + E \cdot x_{dest.sh}$

Table 3: Energy and Exergy Destruction Equations for the TECARP System

Component	Energy is Different from Exergy	Exergy Balance
Pump 1	$W_{p1} = m_2(h_3 - h_2)$	$E \cdot x_2 + W_{p1} = E \cdot x_3 + E \cdot x_{dest.pump1}$
Solution heat exchanger 1	$m_5 h_5 + m_{22} h_{22} = m_4 h_4 + m_6 h_6$	$E \cdot x_5 + E \cdot x_{22} = E \cdot x_4 + E \cdot x_6 + E \cdot x_{dest.shx1}$
Absorber 1	$m_7 h_7 + m_{26} h_{26} = m_2 h_2 + Q_{Abs1}$	$E \cdot x_7 + E \cdot x_{26} + E \cdot x_{cw2.in} = E \cdot x_2 + E \cdot x_{cw2.out} + E \cdot x_{dest.Abs1}$
Generator 1	$m_4 h_4 + m_2 1 h_2 1 + Q_{con2} + QAbs2 = m_5 h_5 + m_8 h_8 + Q_{Gen1}$	$E \cdot x_4 + E \cdot x_{21} + E \cdot x_{con2} + E \cdot x_{Abs2} = E \cdot x_5 + E \cdot x_8 + E \cdot x_{dest.Gen1}$
Condenser 1	$m_9 h_9 + m_1 1 h_1 1 = m_1 0 h_1 0 + Q_{con1}$	$E \cdot x_9 + E \cdot x_{11} + E \cdot x_{cw1.in} = E \cdot x_{10} = E \cdot x_{cw1.out} + E \cdot x_{dest.con2}$
Pump 2	$W_{p2} = m_{12}(h_{13} - h_{12})$	$E \cdot x_{12} + W_{p2} = E \cdot x_{13} + E \cdot x_{dest.pump2}$
Solution heat exchanger 2	$m_{15} h_{15} + m_{24} h_{24} = m_{14} h_{14} + m_{16} h_{16}$	$E \cdot x_{15} + E \cdot x_{24} = E \cdot x_{14} + E \cdot x_{16} + E \cdot x_{dest.shx2}$
Generator 2	$m_{14} h_{14} + m_{23} h_{23} + m_{sh} h_{hs.int} = m_{15} h_{15} + m_{18} h_{18} + m_{sh} h_{hs.out} + Q_{Gen2}$	$E \cdot x_{14} + E \cdot x_{23} + E \cdot x_{hs.int} = E_{15} + m_{18} + E \cdot x_{hs.out} + E \cdot x_{dest.Gen2}$
Condenser 2	$Q_{con2} = m_{19}(h_{19} - h_{20})$	$E \cdot x_{19} + E \cdot x_{cw4.in} = E \cdot x_{20} + E \cdot x_{cw4.out} + E \cdot x_{dest.con2}$
Rectifier 1	$m_3 h_3 + m_8 h_8 = m_9 h_9 + m_{21} h_{21} + m_{22} h_{22} + Q_{Rec1}$	$E \cdot x_3 + E \cdot x_8 = E \cdot x_9 + E \cdot x_{21} + E \cdot x_{22} + E \cdot x_{dest.Rec1}$
Rectifier 2	$m_{13} h_{13} = m_{30} h_{30} = m_{19} h_{19} + m_{23} h_{23} + m_{24} h_{24} + Q_{Rec2}$	$E \cdot x_{13} + E \cdot x_{30} = E \cdot x_{19} + E \cdot x_{23} + E \cdot x_{24} + E \cdot x_{dest.Rec2}$
Evaporator	$Q_{Eva} = m_{25}(h_1 - h_{25})$	$E \cdot x_{25} + E \cdot x_{cf.in} = E \cdot x_1 + E \cdot x_{cf.out} + E \cdot x_{dest.Eva}$
Refrigerant sub-cooler	$m_1 h_1 + m_{10} h_{10} = m_{28} h_{28} + m_{29} h_{29}$	$E \cdot x_1 + E \cdot x_{10} = E \cdot x_{28} + E \cdot x_{29} + E \cdot x_{dest.Rsc}$
Expander	$W_{Exp} = m_{32}(h_{33} - h_{32})$	$E \cdot x_{32} = E \cdot x_{33} + W_{Exp} + E \cdot x_{dest.Exp}$
Compressor	$W_{Com} = m_{29}(h_{34} - h_{29})$	$E \cdot x_{29} + W_{Com} = E \cdot x_{34} + E \cdot x_{dest.Com}$
Absorber 2	$m_{17} h_{17} + m_{27} h_{27} = m_{12} h_{12} + Q_{Abs1}$	$E \cdot x_{17} + E \cdot x_{27} + E \cdot x_{cw3.in} = E \cdot x_{12} + E \cdot x_{cw3.out} + E \cdot x_{dest.Abs2}$
Super heater	$Q_{sh} = m_{31}(h_{32} - h_{31})$	$E \cdot x_{31} + E \cdot x_{hs.in} = E \cdot x_{32} + E \cdot x_{hs.int} + E \cdot x_{dest.sh}$

Table 4: Assumed Input Parameters for the Simulation of the 3 Systems

Parameter	SECARP	DECARP	TECARP
Total mass flow rate (kg/s)	1	1	1
Solution heat exchanger and Refrigerant sub-cooler effectiveness	0.85	0.85	0.85
Pump and compressor efficiency	0.80	0.80	0.80
Expander efficiency	0.85	0.85	0.85
Condenser and Absorber temperature ($\circ C$)	35	35	35
Evaporator exit temperature ($\circ C$)	-10	-10	-10
Cooling water inlet/outlet temperature ($\circ C$)	30/35	30/35	30/35
Chilled fluid (ethelyne) inlet/outlet temperature ($\circ C$)	-1/-10	-1/-10	-1/-10
Refrigerant separation ratio	$\frac{m_{19}}{m_7}$	$\frac{m_{32}}{m_7}$	$\frac{m_{31}}{m_{18}}$
Solution circulation ratio	$\frac{X_9 - X_4}{X_3 - X_4}$=9	$\frac{X_{24} - X_{19}}{X_{18} - X_{19}}$=19	$\frac{X_{19} - X_{15}}{X_{14} - X_{15}}$=30

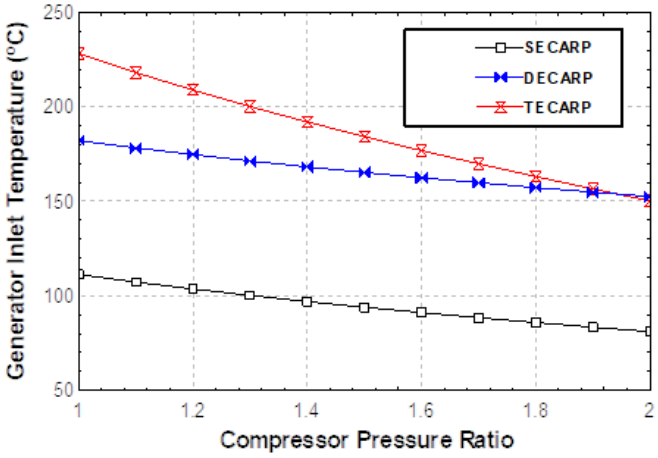

Figure 4: Effect of Compression Ratio on the Generator Inlet Temperatures

4 Results and Discussion

The inclusion of the compressor in these systems is to enable them operate at lower temperatures compared to the traditional vapor absorption cycles. As explained earlier, the power consumption of the pumps and the compressors in all three systems is provided by expander output power . For each of the systems to be self-sufficient, the amount of the refrigerant separated for the turbine operation has to exactly what would be needed to power the compressors and pumps. This will be determined by the refrigerant split ratio (RSR) of the respective systems. All the power generated is consumed by the solution pump and compressor.

As the compression pressure ratio Prcom increases, the mechanical compression process enhances the heat transformation process. Consequently, the required driving heat source temperature 'ths,in' drops when the Prcom increases, as shown in Fig. 4. In the TECARP system, as Prcom increases from 1 to 2, the generator inlet temperature reduces from $228°C$) to $150°C$)in the TECARP system, representing a 34.78% decrease. In comparison, the SECARP system experiences a 21.73% decrease in the generator temperature while the decrease in the DECARP system is 16.25%.

Fig. 5 shows the effect of increasing the Prcom on the compression work in all three systems. As expected, when the Prcom increases from 1 to 2, the compression work in the systems also increases. The figure shows that at Prcom = 1, the compression work in all three systems is zero but as the pressure ratio increases, the value also increases up to the final values of about 6 kW, 7 kW, and 7.5 kW in the SECARP, DECARP, and TECARP systems respectively.

Figure 6 also shows the amount of vapour that needs to be produced by the generator in order for the system to run on its own, that is, to power the solution pump and mechanical compressor.. This figure shows that as Prcom increases, the RSR also increases in all three systems. This is because the systems will require more refrigerant for power production to cover the increasing compression work as shown in Fig. 5. However, it is observed that the RSR to ensure autonomous operation in the TECARP system starts from about 0.22 and increases to about 0.79 as the Prcom increases. This is as a result of the design arrangement of the TECARP system in which the refrigerant is extracted from the exit of the high pressure generator where the mass flow rate is low.

Fig. 7 shows the energetic implications of the compression process on the three cycles. The cooling output of the cycles decrease as the Prcom increases from 1 to 2. The cooling load of the SECARP and DECARP systems reduce as the Prcom increases. This is because the RSR also has to increase to cover for the increasing compression work. The cooling load of the TECARP system is however hardly affected as shown in the figure. This is because of the design of the TECARP system where the inner cycle is unaffected by the refrigerant extraction for power generation and since majority of the refrigerant that goes into the evaporator comes from the inner cycle, the cooling load will be hardly affected.

In reality the cooling systems often serve fixed loads, so they have to supply the same amount of cooling throughout their operation. Also, for the solar powered systems that are being considered in this study, intermittent heat supply associated with solar thermal systems can be a problem for fixed load supply. These systems should therefore be able to adjust its heat source temperature requirements to produce the same cooling load by adjusting the Prcom. Fig. 8a, 8b, 8c show the effect of pressure ratio increase in the SECARP, DECARP, and TECARP systems respectively. The cooling loads in each system has been fixed as 60 kW and 75 kW. The effect on the generator inlet temperatures and the RSR in the systems are illustrated. The figures show that for the 3 cycles, the 60 kW systems require less operating generator temperatures affirming that the operating temperature increases as the system size increases. However, the RSR is more in the 60 kW systems as they have to compensate for less amount of refrigerant from the generators compared to the 75 kW systems.

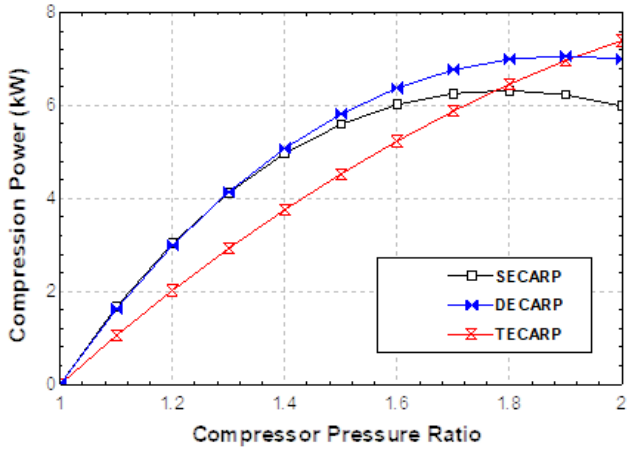

Figure 5: Effect of Compression Ratio on the Compression Power

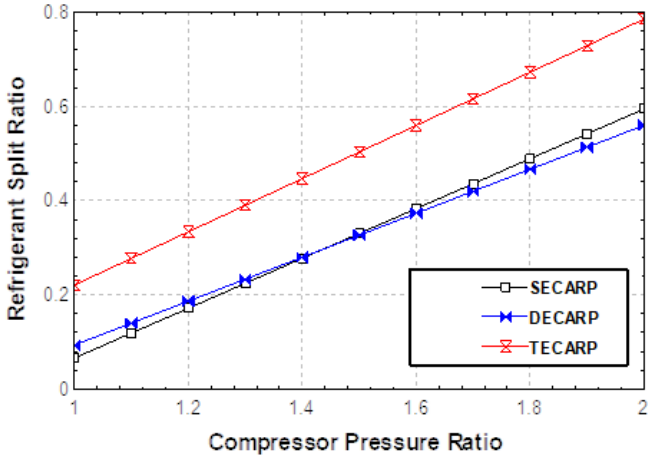

Figure 6: Effect of Compression Ratio on the Refrigerant Split Ratio (RSR) Required for Self-Sufficiency

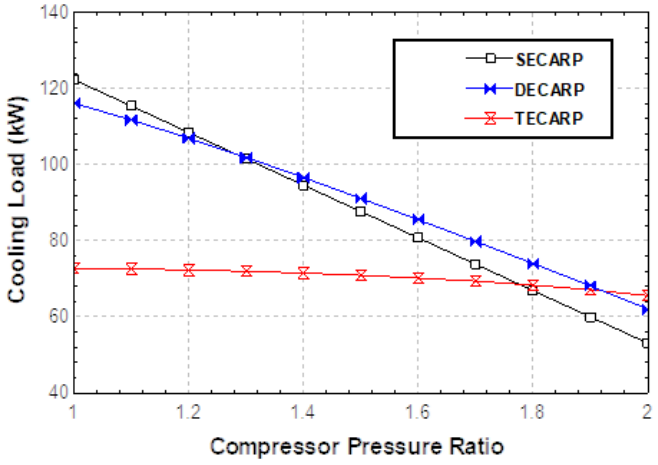

Figure 7: Effect of Compression Ratio on the Cooling Loads

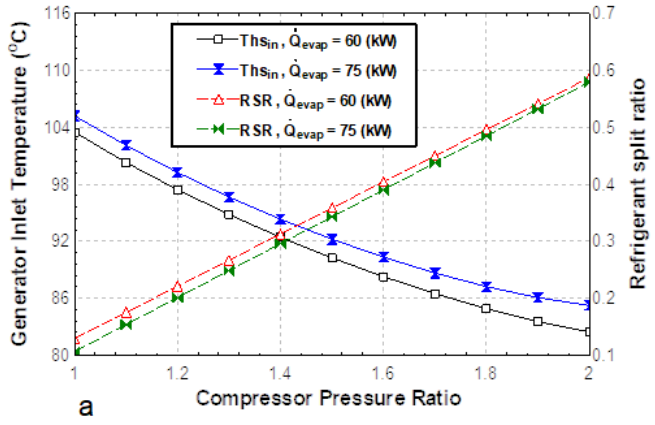

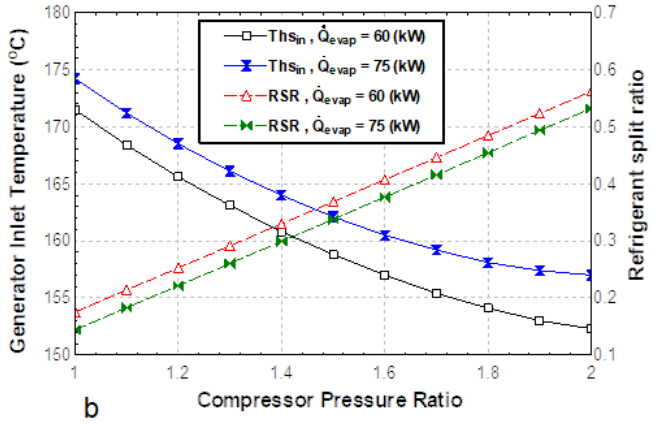

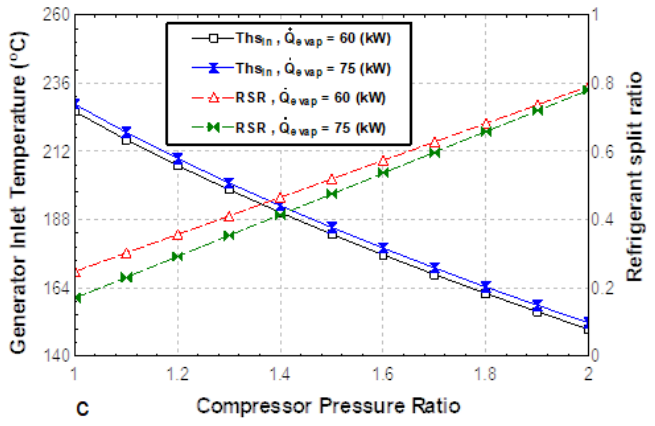

Figure 8: Effect of the Compression Pressure Ratio on the Generator Inlet Temperature and the RSR in (a) – SECARP (b) – DECARP (c) – TECARP for Fixed Cooling Loads

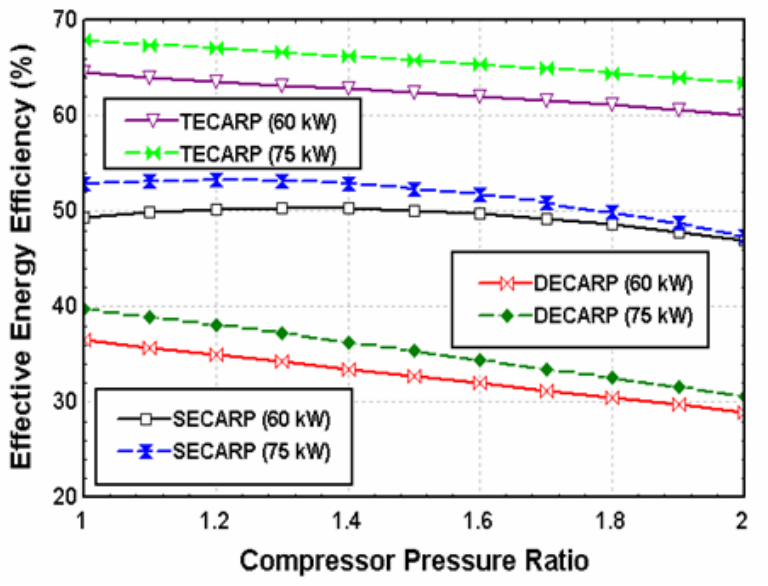

Figure 9: Effect of the Compressor Pressure Ratio on the Effective Energy Efficiency for Fixed System Sizes of the Three Cycles

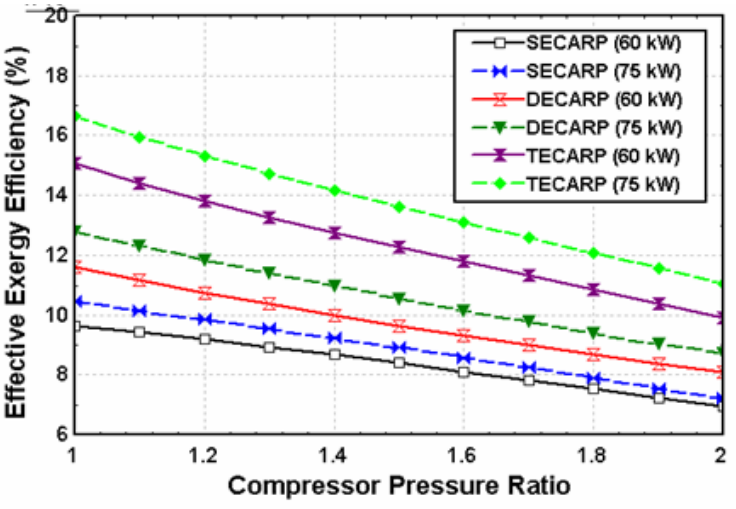

Figure 10: Effect of the Compressor Pressure Ratio on the Effective Exergy Efficiency for Fixed System Sizes of Three Cycles

Fig. 9 and Fig. 10 show the effect of varying the compression ratio on the effective energy and exergy efficiencies respectively. As the Prcom increases from 1 to 2, the performance of all the 3 systems reduce. The DECARP system can be seen to perform better than the SECARP system when comparing their effective energy efficiencies but the SECARP system performs better in terms of effective exergy efficiency. However, it is observed that the performance of the TECARP system increases as the Prcom increases. The performance of the TECARP system also decreases as the Prcom increases. Both the effective energy and exergy efficiencies decrease with increase in Prcom. The figures also show that the performance of the 75 kW system is better in all the 3 systems.

Fig.11 shows the share of the exergy destruction of each of the components in each of the three systems at Prcom = 2 for 75 kW cooling load. The combined destruction rate is taken for 2 of the same component in a system. e.g. for the 2 condensers in the TECARP system. In this figure, it can be observed that exergy destruction in the absorber is highest for all the systems. The main reason for this is the mass transfer between the internal streams, as well as the heat transfer that takes place between the NH_3/H_2O working fluid pair and the external cooling water circuit. The relatively lower exergy destruction contribution in the generators are due to the assumed perfect thermal capacitance match between the heat source fluid and the NH_3/H_2O mixture in the generator, which minimizes exergy destruction.

The summary of the results obtained from the simulation of the three systems for 75 kW cooling load and Prcom = 2 is

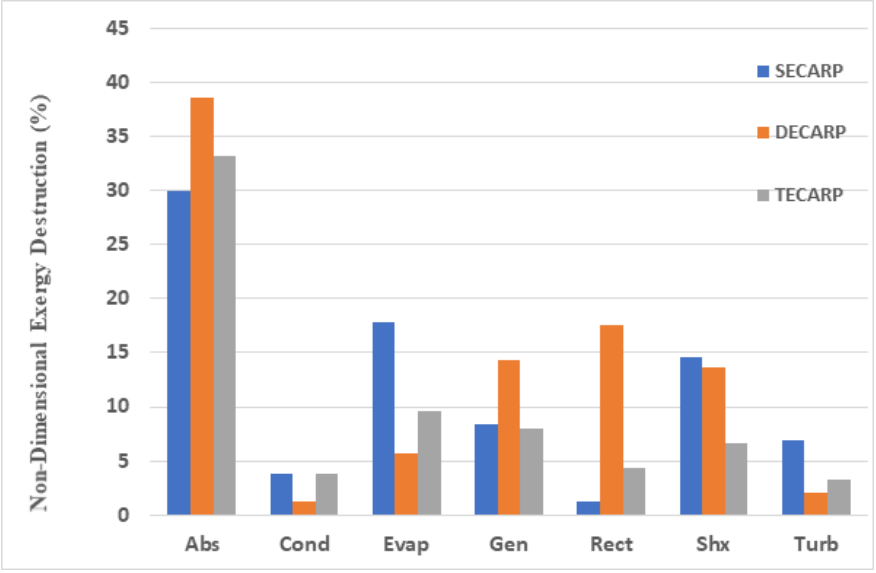

Figure 11: Non-Dimensional Exergy Destruction for Major Components in the 75 kW Systems at Prcom=2

Table 5: System Output Results for the Three Systems at Prcom = 2 and 75 kW Cooling Load

Parameter	SECARP	DECARP	TECARP
Pump1 work (kW)	1.245	1.245	0.9967
Pump2 work (kW)	-	1.197	0.809
Compressor work (kW)	8.461	8.792	8.594
Expander work output (kW)	9.749	11.24	10.49
Absorber1 heat load (kW)	252.7	190	110.9
Absorber2 heat load (kW)	-	128.9	91.8
Condenser1 heat load (kW)	74.18	77.1	65.71
Condenser2 heat load (kW)	-	-	9.318
SHX1 heat load (kW)	140	230	128.4
SHX2 heat load (kW)	-	186	22.94
RSC heat load (kW)	7.203	7.485	7.319
Generator1 load (kW)	244.6	175.5	101.1
Generator2 load (kW)	-	190.4	89.13
Rectifier1 heat load (kW)	5.001	14.31	4.327
Rectifier2 heat load (kW	-	46.62	74.93
Super heater heat load (kW)	3.233	12.6	1.433
Cooling exergy (kW)	5.524	5.74	5.611
Heat source input exergy, $\Delta(Ex)_{hs}$ (kW)	38.16	60.68	35.95
Effective energy efficiency (%)	7.5	9.2	20.8
Effective exergy efficiency (%)	48.4	30.8	52.3

presented in Table 5. The state point properties for each of the three systems are also presented in Tables 6-8.

4.1 Comparison of the Systems with Similar Studies in Literature

The modification of vapor absorption systems with either an expander, a compressor, or a combination of both have been previously studied by various researchers. The expander integration provides added power generation from the vapor absorption system to cover power needs when necessary. In its case, the integration of the compressor helps to reduce the inlet temperature required for the fluid separation in the generator. A combination of the two gives a hybrid system capable of providing both cooling/refrigeration and power generation and at a lower operating temperature. The three systems evaluated in this study are compared to other modified systems in literature as presented in Table 9.

The systems selected for the comparison have either an integrated expander, compressor, or both. The effective performance of the systems with the integrated expander are listed in the table while the inlet temperature reduction achieved for the systems with integrated compressors are listed. The systems with both integrated compressor and expander therefore have both the inlet temperature reduction and the performances listed.

The results show that the systems with integrated expanders are able to operate on high pressure ratios (3.5-4) which results in a high effective exergy efficiency $(\sim 42\%)$ for the single and triple effect hybrid systems operating on $NH_3 - H_2O$. On the other hand, the systems with integrated compressors are able to reach pressure ratios of around 2. The single effect $NH_3 - LiNO_3$ system showed a $24^\circ C$ inlet temperature reduction. In comparison, the single effect hybrid $NH_3 - H_2O$ system presented in this study has a $31^\circ C$ temperature reduction and an effective exergy efficiency of 48.4%.

Table 6: Thermodynamic Properties of the SECARP System at Prcom = 2 and 75 kW Cooling Load

State	$T°C$	P (kPa)	$\dot{m}(kg/s)$	x	h (kJ/kg)	s (kJ/kg.K)	$\dot{E}x(kW)$
1	35	556.1	1	0.5562	-78.14	0.366	39.66
2	35.13	1350	1	0.5562	-76.9	0.3668	40.66
3	67.09	1350	1	0.5562	72.16	0.8263	52.7
4	79.94	1350	0.8476	0.4772	121.8	0.9844	32.33
5	43.65	1350	0.8476	0.4772	-43.35	0.491	17.03
6	43.79	556.1	0.8476	0.4772	-43.35	0.494	16.26
7	66.97	1350	0.1532	0.9936	1394	4.535	55.55
8	66.97	1350	0.000782	0.5562	69.3	0.818	0.04094
9	47.22	1350	0.06361	0.999	1332	4.346	22.68
10	35	1350	0.06361	0.999	165.6	0.5802	19.94
11	11.35	1350	0.06361	0.999	52.32	0.1982	19.98
12	-11.07	278.1	0.06361	0.999	52.32	0.2186	19.59
13	-10	278.1	0.06361	0.999	1231	4.694	9.695
14	26.26	278.1	0.06361	0.999	1344	5.102	9.164
15	89.02	556.1	0.06361	0.999	1477	5.177	16.21
16	37.13	1350	1	0.5562	-67.83	0.3961	40.99
17	49.27	556.1	0.1524	0.9959	1386	4.912	36.97
18	66.97	1350	0.0644	0.9936	1394	4.535	23.35
19	66.97	1350	0.08882	0.9936	1394	4.535	32.2
20	80.24	1350	0.08882	0.9936	1430	4.639	32.68
21	30.69	556.1	0.08882	0.9936	1321	4.703	21.24

Table 7: Thermodynamic Properties of the DECARP System at Prcom = 2 and 75 kW Cooling Load

State	$T°C$	P (kPa)	$\dot{m}(kg/s)$	x	h (kJ/kg)	s (kJ/kg.K)	$\dot{E}x(kW)$
1	35	556.1	1	0.419806	-76.653	0.381	7.037
2	35.1	1349.8	1	0.419806	-75.4081	0.383	7.982
3	86.4	1349.8	1	0.419806	154.5751	1.072	32.3
4	101.2	1349.8	0.921843	0.369599	231.2098	1.268	36.67
5	45.2	1349.8	0.918253	0.369599	-19.2477	0.544	4.808
6	45.3	556.1	0.918253	0.369599	-19.2477	0.547	4.013
7	90.8	1349.8	0.14841	0.971023	1481.799	4.784	55.19
8	90.8	1349.8	0.003355	0.419805	175.0014	1.129	0.1204
9	47.2	1349.8	0.066101	0.999	1331.602	4.346	23.57
10	35	1349.8	0.066101	0.999	165.5233	0.58	20.71
11	11.35	1350	0.06361	0.999	52.32	0.1982	19.98
12	-11.1	278.1	0.066101	0.999	52.28945	0.218	20.36
13	-10	278.1	0.066101	0.999	1231.206	4.695	10.07
14	26.3	278.1	0.066101	0.999	1344.44	5.102	9.523
15	88.1	556.1	0.063308	0.983772	1492.155	5.224	16.17
16	101.2	556.1	1.040555	0.208758	292.2798	1.326	37.75
17	101.3	1349.8	1.040555	0.208758	293.4297	1.327	38.76
18	139.4	1349.8	1.044145	0.209311	471.3539	1.778	83.99
19	151.7	1349.8	0.977247	0.158551	546.0175	1.907	91.5
20	109.1	1349.8	0.977247	0.158551	355.685	1.435	42.98
21	112.2	556.1	0.977247	0.158551	355.685	1.438	42.29
22	138.8	1349.8	0.087367	0.777087	1813.496	5.516	38.76
23	138.8	1349.8	0.020469	0.209311	461.3503	1.754	1.594
24	101.2	1349.8	0.066898	0.950816	1530.361	4.911	25.31
25	89	556.1	0.066101	0.999	1477.444	5.177	16.84
26	88.1	556.1	0.081747	0.983772	1492.155	5.224	20.89
27	101.3	1349.8	1.044145	0.209311	293.2158	1.327	38.92
28	101.2	1349.8	0.00359	0.369599	231.2098	1.268	0.1428
29	45.3	556.1	0.063308	0.983772	1349.522	4.799	15.16
30	101.2	1349.8	0.918253	0.369599	231.2098	1.268	36.53
31	90.8	1349.8	0.069456	0.971023	1481.799	4.784	25.83
32	90.8	1349.8	0.078954	0.971023	1481.799	4.784	29.36
33	152.6	1349.8	0.078954	0.971023	1641.361	5.189	32.44
34	87.3	556.1	0.078954	0.971023	1504.471	5.257	20.04
35	88.1	556.1	0.145055	0.983772	1492.155	5.224	36.84

Table 8: Thermodynamic Properties of the TECARP System at Prcom = 2 and 75 kW Cooling Load

State	$T°C$	P (kPa)	$\dot{m}(kg/s)$	x	h (kJ/kg)	s (kJ/kg.K)	$\dot{E}x(kW)$
1	-10.03	277.7	0.06461	0.999	1231	4.695	9.827
2	35	555.4	1	0.5559	-78.19	0.3659	39.54
3	35.08	1350	1	0.5559	-77.2	0.3659	40.54
4	64.04	1350	1	0.5559	55.56	0.7775	50.59
5	70.98	1350	0.9451	0.5302	83.86	0.8682	43.75
6	41.34	1350	0.9451	0.5302	-52.04	0.4553	31.65
7	39.13	555.4	0.9451	0.5302	-52.04	0.4584	30.79
8	67.02	1350	0.05558	0.9936	1394	4.536	20.15
9	47.22	1350	0.0549	0.999	1332	4.346	19.57
10	35	1350	0.06461	0.999	165.6	0.5805	20.24
11	35.01	1350	0.009713	0.999	340.1	1.145	3.103
12	69.04	555.4	0.2525	0.3555	89	0.8678	3.489
13	69.34	3252	0.2525	0.3555	92.2	0.8678	4.298
14	150.6	3252	0.2525	0.3555	479.8	1.879	26.03
15	156.1	3252	0.2428	0.3298	505.4	1.93	26.25
16	137	3252	0.2428	0.3298	411	1.704	19.61
17	92.4	555.4	0.2428	0.3298	411	1.757	15.83
18	150	3252	0.05315	0.8897	1665	4.842	27.64
19	73.91	3252	0.009713	0.999	1300	3.923	4.379
20	69.04	3252	0.009713	0.999	340.1	1.107	3.214
21	67.02	1350	0.000678	0.5559	69.46	0.8186	0.0354
22	36.03	1350	1	0.5559	-72.87	0.38	40.69
23	150	3252	0.001986	0.3555	470.7	1.858	0.1994
24	133.6	3252	0.2525	0.3555	388.9	1.661	19.53
25	-11.1	277.7	0.06461	0.999	52.28	0.2185	19.9
26	95	555.4	0.0549	0.999	1492	5.216	14.12
27	95	555.4	0.009713	0.999	1492	5.216	2.498
28	11.34	1350	0.06461	0.999	52.28	0.198	20.29
29	26.26	277.7	0.06461	0.999	1344	5.103	9.295
30	150	3252	0.0117	0.8897	1665	4.842	6.084
31	150	3252	0.04145	0.8897	1665	4.842	21.56
32	161.6	3252	0.04145	0.8897	1699	4.922	22
33	83.07	555.4	0.04145	0.8897	1446	5.046	9.985
34	89.02	555.4	0.06461	0.999	1477	5.177	16.45
35	95	555.4	0.1061	0.9563	1465	5.139	26.13

Table 9: Comparison of Hybrid Absorption Cooling Systems

Integrated Absorption System	Working Fluid	Reference	Prcom	Temperature Reduction $\delta T_{hs,in}$	Effective Energy Efficiency (%)	Effective Exergy Efficiency (%)
Single effect-expander	$NH_3\ H_2O$	[15]	4	-	7	42
Double effect-expander	$NH_3\ H_2O$	[28]	3.5	-	16.8	42.7
Triple effect–expander	$NH_3\ H_2O$	[28]	3.5	-	14.6	41.8
Single effect-compressor	$NH_3\ LiNO_3$	[29]	2	24	-	-
Triple effect–compressor-expander	$LiBr\ H_2O$	[6]	2.2	50	-	-
Single effect–compressor–expander	$NH_3\ H_2O$	Present study	2	31	7.5	48.4
Double effect–compressor–expander	$NH_3\ H_2O$	Present study	2	29	9.2	30.8
Triple effect–compressor–expander	$NH_3\ H_2O$	Present study	2	78	20.8	52.3

The triple effect compressor-absorber hybrid system operating on $LiBr - H_2O$ was able to provide a $50°C$ inlet temperature reduction. The triple effect $NH_3 - H_2O$ hybrid system presented in this study can provide a $78°C$ inlet temperature reduction and its effective exergy efficiency reaches 52.3%. This shows the large benefits that the hybrid triple effect systems can gain in comparison to the other systems, especially in terms of the inlet temperature reduction.

5 Conclusion

This research analyses three compressor-assisted absorption cycles for refrigeration and power using ammonia water as working fluid. The conclusions are as follows :

- The incorporation of a compressor to the three systems result in the heat source temperature (ths,in) reducing in all the systems. Increasing the compression ratio from 1 to 2 reduces 'ths,in' in the SECARP system from $111.3°C$ to $81.1°C$ representing a 27% reduction. The reduction in the DECARP system is from $182.1°C$ to $152.5°C$ representing a 16% and the temperature in the TECARP system drops from $228.3°C$ to $150.3°C$ representing a 34% reduction.
- The refrigerant split ratio (RSR) needed to ensure self-sufficiency in the TECARP system increases from 0.22 to 0.79. This is significantly higher compared to the SECARP and DECARP systems.
- The performance analysis of the systems shows that the TECARP system experience a much bigger benefit from integrating the compressor in the system. The results show that while the energetic and exergetic performance of the SECARP and DECARP systems reduce as the Prcom increases, the TECARP system's performance increases with

increase in Prcom.

- The exergy analysis of the systems reveal that the largest destruction rate occurs in the absorbers of each of the three systems. Also, the absorber in the DECARP system experiences the highest exergy destruction.

This study may provide a new efficient way to produce low-temperature heat source to provide power and cooling by using mid-temperature heat sources. The systems analyzed can utilize heat from a solar thermal collector for instance to provide both cooling and power when needed. The option of self-sufficiency in the cooling mode of the systems also make them prime candidates for operation in remote locations where grid electricity may be non-existent. Analysis of the systems show that the TECARP system will be most suitable for this application as it offers the biggest inlet operating temperature reduction and the best performance of the three systems.

Acknowledgment

The authors would like to acknowledge Cyprus Science University, Brunei Darussalam University, International Cyprus University and National University of Sciences and Technology.

Authors' Contributions

In this study, all authors studied and designed the article.

Competing Interests

The authors declare that they have no conflict of interest.

References

[1] Molly, "Proof of climate change: How do we cool a heating world?," Sept. 2018.
[2] H. Chua, H. Toh, A. Malek, K. Ng, and K. Srinivasan, "A general thermodynamic framework for understanding the behaviour of absorption chillers," *International Journal of Refrigeration*, vol. 23, no. 7, pp. 491–507, 2000.
[3] S. A. Khan, "Comparative analysis of single and double effect libr-water absorption system," in *4th International Conference on Recent Innovations in Sciences Engineering and Management*, 2016.
[4] Minnesota Pollution Control Agency, "Chlorofluorocarbons (cfcs) and hydrofluorocarbons (hfcs)."
[5] J. Wang, B. Wang, W. Wu, X. Li, and W. Shi, "Performance analysis of an absorption-compression hybrid refrigeration system recovering condensation heat for generation," *Applied Thermal Engineering*, vol. 108, pp. 54–65, 2016.
[6] G. Shu, J. Che, H. Tian, X. Wang, and P. Liu, "A compressor-assisted triple-effect h2o-libr absorption cooling cycle coupled with a rankine cycle driven by high-temperature waste heat," *Applied Thermal Engineering*, vol. 112, pp. 1626–1637, 2017.
[7] V. H. F. Flores, J. C. Román, and G. M. Alpírez, "Performance analysis of different working fluids for an absorption refrigeration cycle," *American Journal of Environmental Engineering, DOI*, vol. 10, pp. 1–10, 2014.
[8] J. Deng, R. Wang, and G. Han, "A review of thermally activated cooling technologies for combined cooling, heating and power systems," *Progress in energy and combustion science*, vol. 37, no. 2, pp. 172–203, 2011.
[9] V. Eveloy and D. S. Ayou, "Sustainable district cooling systems: Status, challenges, and future opportunities, with emphasis on cooling-dominated regions," *Energies*, vol. 12, no. 2, p. 235, 2019.
[10] A. Shirazi, R. A. Taylor, G. L. Morrison, and S. D. White, "Solar-powered absorption chillers: A comprehensive and critical review," *Energy conversion and management*, vol. 171, pp. 59–81, 2018.
[11] J.-S. Kim, F. Ziegler, and H. Lee, "Simulation of the compressor-assisted triple-effect h2o/libr absorption cooling cycles," *Applied Thermal Engineering*, vol. 22, no. 3, pp. 295–308, 2002.
[12] M. Udayakumar *et al.*, "Studies of compressor pressure ratio effect on gaxac (generator–absorber–exchange absorption compression) cooler," *Applied Energy*, vol. 85, no. 12, pp. 1163–1172, 2008.
[13] W. Chen *et al.*, "Investigation of [mmim]dmp/ch3oh absorption refrigeration thermodynamic performances," *Journal of Engineering Thermophysics*, vol. 34, pp. 689–693, 2013.
[14] D. Boer, M. Valles, and A. Coronas, "Performance of double effect absorption compression cycles for air-conditioning using methanol–tegdme and tfe–tegdme systems as working pairs: Performances de cycles à compression absorption à double effet pour le conditionnement d'air utilisant les couples méthanol–tegdme ou tfe–tegdme," *International Journal of Refrigeration*, vol. 21, no. 7, pp. 542–555, 1998.
[15] G. Demirkaya, R. Vasquez Padilla, D. Y. Goswami, E. Stefanakos, and M. M. Rahman, "Analysis of a combined power and cooling cycle for low-grade heat sources," *International Journal of Energy Research*, vol. 35, no. 13, pp. 1145–1157, 2011.
[16] G. P. Kumar, R. Saravanan, and A. Coronas, "Simulation studies on simultaneous power, cooling and purified water production using vapour absorption refrigeration system," *Applied Thermal Engineering*, vol. 132, pp. 296–307, 2018.
[17] S. Aghniaey and S. M. S. Mahmoudi, "Exergy analysis of a novel absorption refrigeration cycle with expander and compressor," *Indian Journal of Scientific Research*, vol. 1, pp. 815–822, 2014.
[18] D. S. Ayou, J. C. Bruno, and A. Coronas, "Integration of a mechanical and thermal compressor booster in combined absorption power and refrigeration cycles," *Energy*, vol. 135, pp. 327–341, 2017.
[19] C. F. Okwose, M. Abid, and T. A. Ratlamwala, "Performance analysis of compressor-assisted two-stage triple effect absorption refrigeration cycle for power and cooling," *Energy Conversion and Management*, vol. 227, p. 113547, 2021.
[20] C. F. Okwose, M. Abid, and T. A. H. Ratlamwala, "Performance evaluation of compressor assisted multi-effect absorption refrigeration cycles for power and cooling using evacuated tube collectors," *International Journal of Exergy*, vol. 32, no. 3, pp. 227–248, 2020.
[21] K. E. Herold, R. Radermacher, and S. A. Klein, *Absorption chillers and heat pumps*. CRC press, 2016.
[22] V. Zare, S. Mahmoudi, and M. Yari, "An exergoeconomic investigation of waste heat recovery from the gas turbine-modular helium reactor (gt-mhr) employing an ammonia–water power/cooling cycle," *Energy*, vol. 61, pp. 397–409, 2013.
[23] R. Misra, P. K. Sahoo, and A. Gupta, "Thermoeconomic evaluation and optimization of an aqua-ammonia vapour-absorption refrigeration system," *International Journal of Refrigeration*, vol. 29, no. 1, pp. 47–59, 2006.
[24] S. Salehi and M. Yari, "Exergoeconomic assessment of two novel absorption-ejection heat pumps for the purposes of supermarkets simultaneous heating and refrigeration using nascn/nh3, lino3/nh3 and h2o/nh3 as working pairs," *International Journal of Refrigeration*, vol. 101, pp. 178–195, 2019.

[25] A. Yıldız and M. A. Ersöz, ‘‘Energy and exergy analyses of the diffusion absorption refrigeration system,’’ *Energy*, vol. 60, pp. 407–415, 2013.
[26] A. Vidal, R. Best, R. Rivero, and J. Cervantes, ‘‘Analysis of a combined power and refrigeration cycle by the exergy method,’’ *Energy*, vol. 31, no. 15, pp. 3401–3414, 2006.
[27] X. Zhang, L. Cai, and T. Chen, ‘‘Energetic and exergetic investigations of hybrid configurations in an absorption refrigeration chiller by aspen plus,’’ *Processes*, vol. 7, no. 9, p. 609, 2019.
[28] D. S. Ayou, J. C. Bruno, and A. Coronas, ‘‘Combined absorption power and refrigeration cycles using low-and mid-grade heat sources,’’ *Science and Technology for the Built Environment*, vol. 21, no. 7, pp. 934–943, 2015.
[29] R. Ventas, A. Lecuona, A. Zacarías, and M. Venegas, ‘‘Ammonia-lithium nitrate absorption chiller with an integrated low-pressure compression booster cycle for low driving temperatures,’’ *Applied Thermal Engineering*, vol. 30, no. 11-12, pp. 1351–1359, 2010.